Holographic magnetized chiral density wave*

Yanyan Bu(卜严严)[2;1)] Shu Lin(林树)[1;2)]

[1] School of Physics and Astronomy, Sun Yat-Sen University, Zhuhai 519082, China
[2] Department of Physics, Harbin Institute of Technology, Harbin 150001, China

Abstract: We explore the end point of the helical instability in a finite density, finite magnetic field background discussed by Kharzeev and Yee. The nonlinear solution is obtained and identified with the (magnetized) chiral density wave phase in the literature. We find there are two branches of solutions, which match the two unstable modes found before. At large chemical potential and magnetic field, the magnetized chiral density wave can be thermodynamically preferred over the chirally symmetric phase and chiral symmetry breaking phase. Interestingly, we find an exotic state with vanishing chemical potential at large magnetic field. We also attempt to clarify the role of anomalous charge in the holographic model.

Keywords: chiral density wave, holography, axial anomaly

PACS: 11.25.Tq, 21.65.Qr, 11.30.Rd **DOI:** 10.1088/1674-1137/42/11/114104

1 Introduction

The ground state of hot and dense QCD matter is one of the key questions in the physics of heavy ion collisions and neutron stars. In the former case, strong magnetic fields can be produced in off-center collisions. In the latter case, strong magnetic fields are believed to exist in the cores of neutron stars. Magnetic fields are known to modify QCD phases in different ways. In the absence of baryon chemical potential, a magnetic field enhances chiral symmetry breaking and reduces the critical temperature, phenomena known as magnetic catalysis [1–3] and inverse magnetic catalysis [4, 5] respectively. At finite quark chemical potential, the QCD phase diagram becomes much enriched. In particular, a variety of inhomogeneous phases appear, including chiral density waves [6], solitonic modulation [7, 8], crystalline color superconductors [9], quarkyonic spirals [10] etc. The quark density is crucial in the formation of these inhomogeneities; see Ref. [11] for a review. The presence of magnetic field tends to widen the inhomogenous phases, leading to magnetized-chiral density waves [12–15] or magnetized kinks [16], magnetized quarkyonic chiral spirals [17] etc.

Interestingly, the interplay of quark density and magnetic field can also lead to more new phases. This is realized through axial anomaly: at low temperature, effective model studies have found inhomogeneous phases including pion domain walls [18, 19], chiral magnetic spirals [20], chiral soliton lattices [21] etc. See Refs. [22, 23] for comprehensive reviews. From the viewpoint of thermodynamics, the formation of inhomogeneous phases induces an anomalous charge, which can lower the free energy of the system [18, 21]. However, the nature of anomalous charge remains a mystery. It is desirable to search for the inhomogeneous phases in other approaches. A number of such studies using holographic models have been carried out [24–30]. In this work, we aim at finding the holographic analog of the magnetized chiral density wave. This work is inspired by early work by Kharzeev and Yee [24], in which they found an unstable helical mode. We will find the end point of the instability and identify it with the magnetized chiral density wave (MCDW) phase. The competition of the MCDW and conventional chiral symmetry breaking phase and restored phase reveals novel structure. We will emphasize the role of anomaly and attempt to clarify the nature of anomalous charge.

The paper is organized as follows. In Section **2**, we give a brief review of the holographic model and the known phase diagram for homogeneous phases [31]. In Section **3**, we present an ansatz for the MCDW phase, solve it numerically and obtain its thermodynamics. We discuss the role of anomalous charge in the MCDW phase in Section **4**. We summarize and discuss future perspectives in Section **5**.

Received 9 July 2018, Published online 28 September 2018

∗ S. L. is supported by One Thousand Talent Program for Young Scholars and NSFC (11675274, 11735007), Y. B. is supported by the Fundamental Research Funds for the Central Universities (122050205032) and the NSFC (11705037)

1) E-mail: yybu@hit.edu.cn

2) E-mail: linshu8@mail.sysu.edu.cn

2 A quick review of the model

The holographic model we use is the D3/D7 model. The model contains N_c D3 branes and N_f D7 branes. The D3 branes generate the AdS black hole background. In the limit $N_f \ll N_c$, the backreaction of D7 branes is suppressed. The field theory dual of the model is a $\mathcal{N}=4$ Super Yang-Mills (SYM) field and $\mathcal{N}=2$ hypermultiplet fields, transforming in adjoint and fundamental representations of the $SU(N_c)$ group respectively. The model is close to QCD in the sense that the $\mathcal{N}=4$ and $\mathcal{N}=2$ fields can be identified as gluons and quarks respectively. The probe limit is analogous to the quenched approximation. The explicit form of the AdS black hole background is given by [32]:

$$\begin{aligned} \mathrm{d}s^2=&-\frac{r_0^2}{2}\frac{f^2}{H}\rho^2\mathrm{d}t^2+\frac{r_0^2}{2}H\rho^2\mathrm{d}x^2+\frac{\mathrm{d}\rho^2}{\rho^2}+\mathrm{d}\theta^2\\ &+\sin^2\theta\mathrm{d}\phi^2+\cos^2\theta\mathrm{d}\Omega_3^2, \end{aligned} \tag{1}$$

where

$$f=1-\frac{1}{\rho^4},\quad H=1+\frac{1}{\rho^4}. \tag{2}$$

We set the AdS radius to 1. The temperature is given by $T=r_0/\pi$. We also parametrize the S_5 coordinates in terms of S_3 coordinates and two other angular coordinates θ and ϕ. The background also contains a nontrivial Ramond-Ramond form

$$\begin{aligned} F_5=&r_0^4\rho^3 Hf\mathrm{d}t\wedge\mathrm{d}x_1\wedge\mathrm{d}x_2\wedge\mathrm{d}x_3\wedge\mathrm{d}\rho\\ &+4\cos^3\theta\sin\theta\mathrm{d}\theta\wedge\mathrm{d}\phi\wedge\mathrm{d}\Omega_3. \end{aligned} \tag{3}$$

The D7 branes occupy the worldvolume of D3 branes. In addition, they occupy the S_3 coordinates. Their position in the x_8–x_9 plane is parametrized by polar coordinates, with radius $\rho\sin\theta$ and angle ϕ. The rotational symmetry in the x_8–x_9 plane corresponds to $U(1)_R$ symmetry in the field theory. Finally, there is an additional $U(1)_B$ symmetry from the worldvolume gauge field of D7 branes. In comparison with QCD, the $U(1)_R$ and $U(1)_B$ symmetries are identified as axial and baryon symmetries respectively.

With the background metric (1), the gluons provide a thermal bath at fixed temperature for quarks. The quark chemical potential and magnetic field are turned on by a nonvanishing $A_t(\rho)$ and constant $F_{xy}=B$. The phase diagram has been obtained by Evans et al [31], showing a rich structure. There is one order parameter of the system, namely the chiral condensate. The condensate is determined by the embedding of D7 branes in the D3 brane background. There are two possible embeddings for D7 branes: black hole embedding and Minkowski embedding, corresponding to the chirally symmetric (χS) phase and chiral symmetry breaking (χSB) phase. The phases can further be classified based on quark number density. For the χS phase, only the finite density state is allowed. For the χSB phase, both finite density and zero density states are allowed. In total, three homogeneous phases are found in Ref. [31]: zero density with χSB phase, finite density with χSB phase, and finite density with χS phase.

The action of D7 branes is given by a Dirac-Born-Infeld (DBI) term and Wess-Zumino (WZ) term

$$\begin{aligned} &S_{D7}=S_{\mathrm{DBI}}+S_{\mathrm{WZ}},\\ &S_{\mathrm{DBI}}=-N_f T_{D7}\int\mathrm{d}^8\xi\sqrt{-\det\left(g_{ab}+2\pi\alpha'\tilde{F}_{ab}\right)},\\ &S_{\mathrm{WZ}}=\frac{1}{2}N_f T_{D7}(2\pi\alpha')^2\int P[C_4]\wedge\tilde{F}\wedge\tilde{F}. \end{aligned} \tag{4}$$

Here T_{D7} is the D7 brane tension. g_{ab} and $\tilde{F}_{ab}$ are the induced metric and worldvolume field strength respectively. Defining

$$\begin{aligned} &F_{ab}=2\pi\alpha'\tilde{F}_{ab},\\ &\mathcal{N}=N_f T_{D7}2\pi^2=\frac{N_f N_c\lambda}{(2\pi)^4}, \end{aligned} \tag{5}$$

we can simplify the action to

$$\begin{aligned} &S_{\mathrm{DBI}}=-\frac{\mathcal{N}}{2\pi^2}\int\mathrm{d}^8\xi\sqrt{-\det(g_{ab}+F_{ab})},\\ &S_{\mathrm{WZ}}=\frac{1}{4\pi^2}\mathcal{N}\int P[C_4]\wedge F\wedge F. \end{aligned} \tag{6}$$

The embedding function θ and worldvolume gauge fields A_t are determined by minimizing the action. The asymptotic behaviors of θ and A_t are given by

$$\sin\theta=\frac{m}{\rho}+\frac{c}{\rho^3}+\cdots,\qquad A_t=\mu-\frac{n}{\rho^2}+\cdots. \tag{7}$$

The coefficients m and c are related to the bare quark mass M_q and chiral condensate $\langle\bar{\psi}\psi\rangle$ as [33] $M_q=\frac{mr_0}{2\sqrt{2}\pi\alpha'}$, $\langle\bar{\psi}\psi\rangle=-\sqrt{2}\pi\alpha'\mathcal{N}cr_0^3$. The coefficients μ and n are related to the quark chemical potential μ_q and quark number density n_q as: $\mu_q=\frac{\mu r_0}{2\pi\alpha'}$, $n_q=2\pi\alpha'\mathcal{N}nr_0^3$. Below we set $r_0=1$. This is equivalent to setting $\pi T=1$.

For the homogeneous phase, the WZ term is not relevant. However, when B and μ are large, the system is found to contain an unstable mode involving simultaneous fluctuations of x_8 and x_9 [24]. It is further conjectured that the end point of this instability is the helical phase. The presence of the WZ term is essential to the instability. In the next section, we will find the end point of the instability and identify it with the MCDW phase known in the literature [13].

3 Magnetized chiral density wave

We start with the following ansatz for the MCDW:

$$A_t=A_t(\rho),\qquad \theta=\theta(\rho),\qquad \phi=kz. \tag{8}$$

The last two equations in Eq. (8) can be written equivalently as

$$x_8+ix_9=\mathrm{e}^{\mathrm{i}kz}\rho\sin\theta(\rho). \tag{9}$$

Note that A_t depends on ρ only. It gives rise to a homogeneous quark number density. The fields x_8 and x_9 form a spiral in the direction parallel to the magnetic field. The limit $k\to 0$ reduces to the homogeneous case studied before. In this limit, $x_8=\rho\sin\theta$ is dual to the chiral condensate:

$$\bar{\psi}\psi\propto c. \tag{10}$$

The ansatz (8) is simply a chiral rotation of chiral condensate along the z direction:

$$\bar{\psi}\psi+i\bar{\psi}i\gamma_5\psi\propto c(\cos kz+i\sin kz). \tag{11}$$

In the presence of non-trivial ϕ, the dual field theory contains the following interaction term for quarks [34, 35]:

$$S_I=-m\bar{\psi}\mathrm{e}^{\mathrm{i}\phi\gamma_5}\psi. \tag{12}$$

The interaction term has no analog in QCD. We are interested in the massless limit, where this term vanishes. Therefore the helical phase corresponds to spontaneous breaking of both chiral symmetry and translational symmetry along z. 1D long range order is known to be washed out by fluctuations in effective models, with the ground state containing only quasi-long range order [36, 37]. In the holographic model, the issue is absent because of suppression of fluctuations in the large N_c limit.

Plugging the ansatz (8) into Eq. (6), we obtain

$$\begin{aligned}
&S=\int \mathrm{d}^4x\mathrm{d}\rho(\mathcal{L}_{\mathrm{DBI}}+\mathcal{L}_{\mathrm{WZ}}),\\
&\mathcal{L}_{\mathrm{DBI}}=\mathcal{N}\frac{-1+\chi^2}{4}\sqrt{2+4B^2+1/\rho^4+\rho^4}\sqrt{\frac{1}{\rho^6+\rho^{10}}\left(1+\rho^4+2k^2\rho^2\chi^2\right)\left(2\rho^4(1+\rho^4)A_t'^2(-1+\chi^2)+(-1+\rho^4)^2(1-\chi^2+\rho^2\chi'^2)\right)},\\
&\mathcal{L}_{\mathrm{WZ}}=-\mathcal{N}BkA_t'(-2\chi^2+\chi^4).
\end{aligned} \tag{13}$$

We have defined $\chi=\sin\theta$. Note that the WZ term depends on the gauge potential C_4. We fix the gauge, following Ref. [24], as

$$C_4=\left(\frac{r_0^2}{2}\rho^2H\right)^2\mathrm{d}t\wedge\mathrm{d}x_1\wedge\mathrm{d}x_2\wedge\mathrm{d}x_3-(\cos^4\theta-1)\mathrm{d}\phi\wedge\mathrm{d}\Omega_3. \tag{14}$$

Another gauge choice has been used in Ref. [35]. The difference in fact does not alter the bulk solutions for the MCDW phase because it only causes a constant shift in the total action $\Delta S=\int\mathrm{d}^4x\mathrm{d}\rho BkAt'=\mathrm{Vol}_4Bk\mu$. Clearly it affects the thermodynamics. Our forthcoming analysis will also support this gauge choice (14). The equations of motion can be derived as

$$\begin{aligned}
&\frac{\delta\mathcal{L}}{\delta\chi}-\frac{\mathrm{d}}{\mathrm{d}\rho}\left(\frac{\delta\mathcal{L}}{\delta\chi'}\right)=0,\\
&\frac{\delta\mathcal{L}}{\delta A_t}-\frac{\mathrm{d}}{\mathrm{d}\rho}\left(\frac{\delta\mathcal{L}}{\delta A_t'}\right)=0.
\end{aligned} \tag{15}$$

Since the action depends on A_t only through its derivative, there is a conserved quantity $\frac{\delta\mathcal{L}}{\delta A_t'}$. It is identified with quark number density n [31]. Consequently, we can use

$$\frac{\delta\mathcal{L}}{\delta A_t'}=n. \tag{16}$$

Throughout the paper, we focus on finite density solutions. It is known that only black hole embedding can support finite density solutions [38]. We search for the MCDW solution by numerically integrating the horizon solution to the boundary. The horizon solution for black hole embedding is obtained analytically as

$$\begin{aligned}
&\chi=c_0+c_2(\rho-1)^2+\cdots,\\
&A_t'=2a_2(\rho-1)+3a_3(\rho-1)^2+\cdots,
\end{aligned} \tag{17}$$

with c_0 and a_2 being two independent parameters. We require that the field strength $F_{\rho t}=A_t'$ vanishes on the horizon. Higher order coefficients in the expansion are expressible in terms of c_0 and a_2. We search for numerical solutions with fixed n, and then scan the parameter n. Since n is invariant along the radial direction, we can use n to fix one of the horizon parameters a_2:

$$2Bc_0^2k-Bc_0^4k+\frac{a_2\sqrt{1+B^2}(1-c_0^2)^2(1+c_0^2k^2)}{\sqrt{(1-a_2^2)(1-c_0^2)(1+c_0^2k^2)}}=n. \tag{18}$$

Note that $\chi=\sin\theta$, thus $0<c_0<1$. For a given set of parameters n, B and k, c_0 is to be determined by the boundary condition $m=0$. In general, the MCDW solution exists for continuous values of k at large n and B. To find out the preferred spiral momentum k, we need to minimize the grand potential. The quark chemical potential is given by bulk integration of A_t'

$$\mu=\int_1^\infty\mathrm{d}\rho A_t'. \tag{19}$$

In practice, we need to tune n and k simultaneously such that μ remains unchanged. This is a numerically challenging task. We are able to achieve 1% percentage accuracy for μ. The grand potential Ω is related to the

Euclidean action as

$$\Omega=\frac{1}{\beta}S^E=-\int \mathrm{d}^3x\mathrm{d}\rho\mathcal{L}=-V\int \mathrm{d}\rho\mathcal{L}. \quad (20)$$

The integration of holographic coordinate ρ contains divergence. We regularize the action by imposing a UV cutoff $\rho=\rho_{\max}$ and renormalize by adding the following counter terms: [39]

$$S_{\text{counter}}=\rho_{\max}^4-\frac{m^2\rho_{\max}^2}{2}+\frac{1}{4}\ln\rho_{\max}(2B^2+k^2m^2). \quad (21)$$

The appearance of k in the counter term for the massive case is not surprising, as k appears as a parameter of the theory according to Eq. (12). There is also a finite counter term for the massive case [33]. The finite counter term does not bother us since we focus on the massless case.

The ground state is to be determined by comparing the free energy of the MCDW phase with those of the known χS phase and χSB phase [31]. The χSB phase appears only at large B, while the χS phase exists for any B and finite μ. The χSB phase can be obtained as a limit $k\to 0$ from the MCDW phase. The χS phase corresponds to the trivial embedding $\chi=0$. The free energy is given by the same expression (20). To compare the free energy of the three phases, we use the free energy of the χS phase as a baseline, i.e. we calculate $\Delta\Omega=\Omega_{\text{MCDW}}-\Omega_{\chi\text{S}}$ for the MCDW phase and $\Delta\Omega=\Omega_{\chi\text{SB}}-\Omega_{\chi\text{S}}$ for the χSB phase. $\Delta\Omega$ of the MCDW phase and χSB phase are at percentage level of $\Omega_{\chi\text{S}}$. For the largest magnetic field $B/(\pi T)^2=15$, $\Delta\Omega$ is less than 1% of $\Omega_{\chi\text{S}}$, making comparison of the free energy more difficult.

In general, we find that MCDW solutions exist in two windows of k at large μ and B. The number of windows coincide with the number of unstable modes [24, 40] in the chirally symmetric background. We find the lowest free energy is usually found near the boundary of either window. We show a typical $\Delta\Omega$-k plot in Fig. 1.

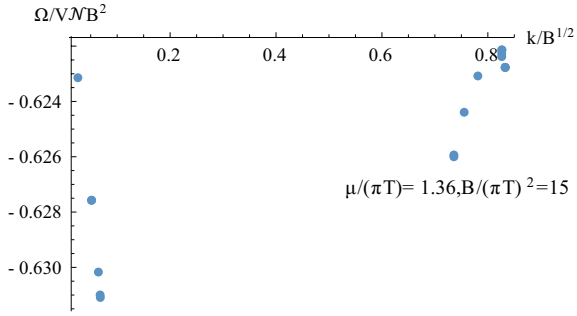

Fig. 1. (color online) $\Omega/\left(V\mathcal{N}B^2\right)$ versus $k/B^{1/2}$ at $B/(\pi T)^2=15$ and $\mu/(\pi T)=1.36$. Here Ω/V is the free energy density with $V=\int \mathrm{d}^3x$. The MCDW phase exists in two branches. The lowest free energy is found at the right-hand boundary of the window of smaller k.

Although there is only one thermodynamically preferred state, we will keep the MCDW states from minimizing free energy in both windows for the purpose of illustration. Below we present three representative MCDW solutions. They include (i) the case with $B/(\pi T)^2=6.5$, where the χSB phase does not exist, and there is competition between the χS phase and MCDW phase; (ii) the case with $B/(\pi T)^2=9$, where the large k branch of the MCDW phase is thermodynamically preferred in a wide region of μ; and (iii) the case with $B/(\pi T)^2=15$, where the small k branch of the MCDW phase is thermodynamically preferred in a wide region of μ.

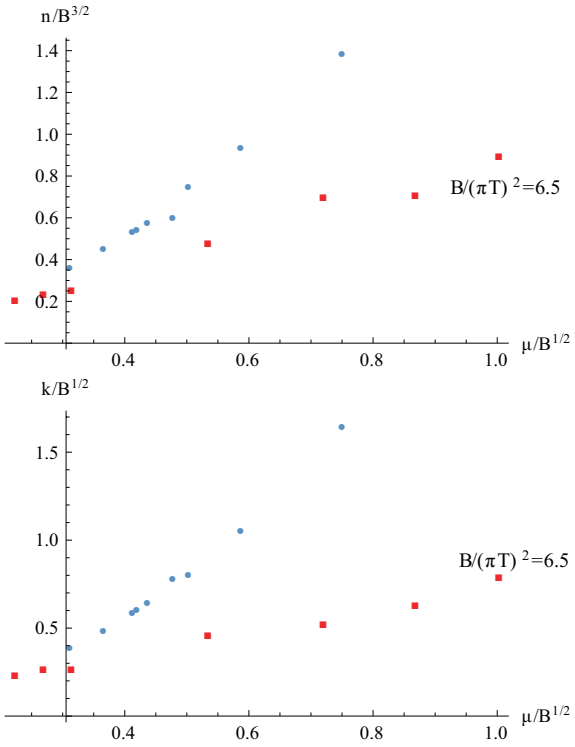

Fig. 2. (color online) $n/B^{3/2}$ versus $\mu/B^{1/2}$ (left) and $k/B^{1/2}$ versus $\mu/B^{1/2}$ (right) at $B/(\pi T)^2=6.5$. The MCDW phase clearly splits into two branches. The branches with large k and small k are marked by blue circles and red squares respectively.

We show the MCDW phase at $B/(\pi T)^2=6.5$ in Fig. 2. For a given μ, there are two MCDW solutions, from the large k branch and small k branch. The large and small k branches of the MCDW solution give large and small density n respectively. The corresponding free energy density $\Delta\Omega/V$ is shown in Fig. 3. At this value of B, the χSB phase does not exist. There is competition between the χS phase and MCDW phase. The large k branch is always thermodynamically more stable than the small k branch, and it dominates over the χS phase when $\mu/B^{1/2}\gtrsim 0.35$.

Next we present the case at $B/(\pi T)^2=9$. In Fig. 4 we show the density and spiral momentum of the two branches of solutions. Again the large and small k branches of the MCDW solution give large and small density n respectively. The comparison of free energy is shown in Fig. 5. We find the MCDW phase with large k

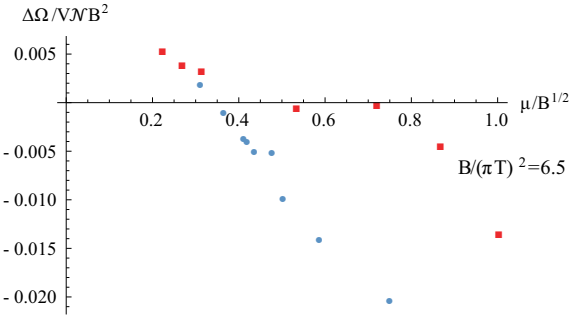

Fig. 3. (color online) $\Delta\Omega/\left(V\mathcal{N}B^2\right)$ versus $\mu/B^{1/2}$ at $B/(\pi T)^2=6.5$ for two branches of MCDW phase, marked by blue circles (large k) and red squares (small k). The large k MCDW phase has lower free energy than the small k MCDW phase at fixed μ. Both are found to have lower free energy than the chirally symmetric phase for large enough μ. In particular, the large k MCDW phase becomes thermodynamically preferred above $\mu/B^{1/2}\simeq 0.35$. The chiral symmetry breaking phase does not exist at this value of B.

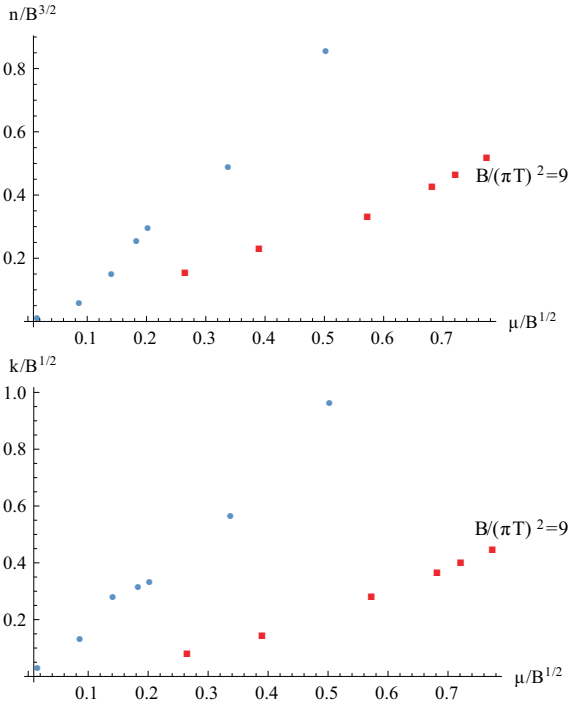

Fig. 4. (color online) $n/B^{3/2}$ versus $\mu/B^{1/2}$ (left) and $k/B^{1/2}$ versus $\mu/B^{1/2}$ (right) at $B/(\pi T)^2=9$. The branches with large k and small k are marked by circles and squares respectively.

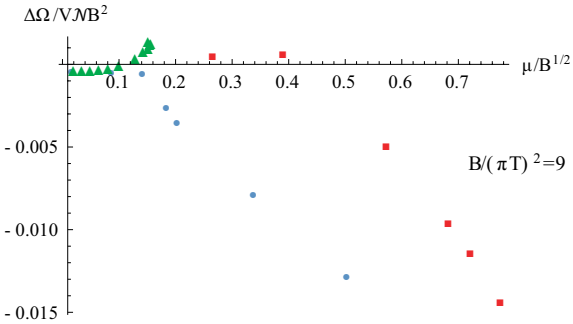

Fig. 5. (color online) $\Delta\Omega/\left(V\mathcal{N}B^2\right)$ versus $\mu/B^{1/2}$ at $B/(\pi T)^2=9$ for two branches of the MCDW phase, marked by blue circles (large k) and red squares (small k), and the χSB phase, marked by green triangles. The large k MCDW phase has lower free energy than the chirally symmetric phase and the small k MCDW phase in their overlap region. The chiral symmetry breaking case exists below a critical value of $\mu/B^{1/2}\simeq 0.15$. The current precision of numerical data does not allow for a decisive conclusion on whether the preferred state is the MCDW or χSB phase.

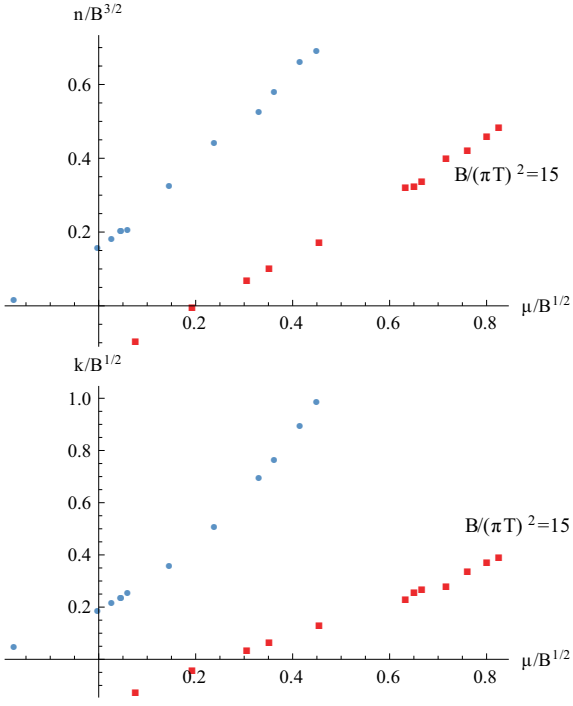

Fig. 6. (color online) $n/B^{3/2}$ versus $\mu/B^{1/2}$ (left) and $k/B^{1/2}$ versus $\mu/B^{1/2}$ (right) at $B/(\pi T)^2=15$. The MCDW phase splits into two branches, marked by blue circles (large k) and red squares (small k). The large k branch of the MCDW phase extends all the way beyond $\mu=0$, indicating that axial anomaly is not necessarily required for its existence. Also, the small k branch extends all the way beyond $n=0(k=0)$. The behavior of n and k follow similar patterns.

is always preferred over the χS phase. At low μ, the χSB phase can occur. Whether the χSB phase can be preferred over the MCDW phase cannot be decisively answered by the current precision of numerical data. Nevertheless, the existence of the χSB phase would be constrained in a narrow window of μ if it exists as a thermodynamically preferred state.

Finally, we present the case of $B/(\pi T)^2 = 15$. In Fig. 6, we show the density and spiral momentum of the two branches of MCDW solutions. While the large/small density and large/small momentum correspondence still holds in general, there are also exotic cases. For the large k branch, the MCDW phase extends below $\mu=0$, i.e. states with negative μ but positive n and k exist. For the small k branch, the MCDW phase extends below $n=0(k=0)$, i.e. states with positive μ but negative n and k exist. By continuity, we can infer that MCDW states with either $\mu=0$ or $k=0$ exist. We also show in Fig. 7 a comparison of the free energy of different phases. The case of $B/(\pi T)^2=15$ is distinct from the cases of $B/(\pi T)^2=6.5$ and $B/(\pi T)^2=9$: the χS phase is never thermodynamically preferred. In the region of large μ, the small k branch of the MCDW phase is preferred. In the region of small μ, the large k branch is preferred. The χSB phase exists in a narrow window in μ. It could be the preferred state in an even narrower window, although the current precision of numerical data does not allow for a decisive answer.

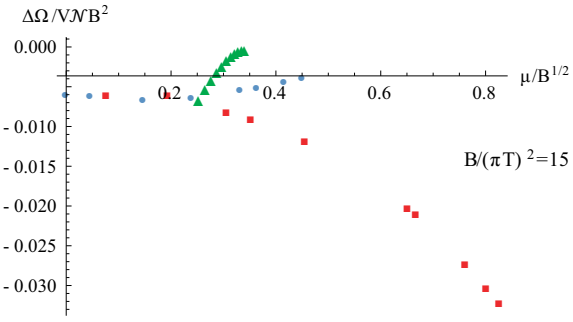

Fig. 7. (color online) $\Delta\Omega/(V\mathcal{N}B^2)$ versus $\mu/B^{1/2}$ at $B/(\pi T)^2=15$ for the two branches of MCDW phase, marked by blue circles (large k) and red squares (small k), and the χSB phase, marked by green triangles. The small k MCDW phase always has lower free energy than the χS phase. The large k MCDW phase might be thermodynamically more favorable in the region of small μ. The χS phase exists in a narrow window of μ. It might be the state with the lowest free energy in an even narrower window. The current precision of numerical data does not allow for a decisive conclusion on whether the preferred state is the MCDW or χSB phase.

4 Anomalous charge and MCDW phase

It is interesting to discuss several aspects of the MCDW phase within the holographic model. We first discuss the role of anomalous charge. In effective models [18], the anomalous charge is generated from a spatially inhomogeneous phase. In the presence of chemical potential, the anomalous charge can lower the free energy of the system: $\Omega\to\Omega-\mu N_{\rm anom}$. Within our holographic model, we can derive the charge density from thermodynamics:

$$\begin{aligned} n=&-\frac{\delta\Omega}{V\delta\mu}=\frac{\int \mathrm{d}\rho\delta\mathcal{L}}{\delta\mu}=\frac{\int \mathrm{d}\rho\delta A_t'\frac{\delta\mathcal{L}}{\delta A_t'}}{\delta\mu}\\ =&\frac{(\delta A_t(\infty)-\delta A_t(1))}{\delta\mu}\frac{\delta\mathcal{L}}{\delta A_t'}. \end{aligned} \tag{22}$$

In the last equality, we use the fact that $\frac{\delta\mathcal{L}}{\delta A_t'}$ is ρ-independent to perform integration over ρ. Note that $A_t(\infty)-A_t(1)=\mu$. We thus obtain

$$n=\frac{\delta\mathcal{L}}{\delta A_t'}=\frac{\delta\mathcal{L}_{\rm DBI}}{\delta A_t'}+\frac{\delta\mathcal{L}_{\rm WZ}}{\delta A_t'}. \tag{23}$$

This is the conserved charge density already used in the previous section. The Lagrangian contains contributions from both DBI and WZ terms. We identify the DBI and WZ contributions as normal and anomalous charge, explicitly:

$$n_{\rm norm}=(\cdots)A_t', \quad n_{\rm anom}=Bk(-2\chi^2+\chi^4). \tag{24}$$

Here $(\cdots)$ is a complicated but positive function of A_t' and χ. In the absence of anomalous charge in the homogeneous phase, it guarantees the charge density has the same sign as the chemical potential. The sign of the anomalous charge is instructive: note that $0<\chi<1$, which gives $n_{\rm anom}>0(n_{\rm anom}<0)$ for $k>0(k<0)$. Indeed, linear stability analysis [24, 40], as well as the full nonlinear solution presented in this work, supports positive k (momentum parallel to magnetic field). This is consistent with the effective model picture in which formation of a spiral generates anomalous charge, lowering the free energy of the system. Had we proceeded with another gauge choice,

$$C_4=\left(\frac{r_0^2}{2}\rho^2 H\right)^2 \mathrm{d}t\wedge\mathrm{d}x_1\wedge\mathrm{d}x_2\wedge\mathrm{d}x_3-\cos^4\theta\mathrm{d}\phi\wedge\mathrm{d}\Omega_3, \tag{25}$$

we would have obtained

$$n_{\rm anom}=Bk(1-\chi^2)^2, \tag{26}$$

therefore $n_{\rm anom}<0(n_{\rm anom}>0)$ for $k>0(k<0)$. It implies that the favorable MCDW phase should be found for $k<0$. This is not consistent with linear stability analysis and nonlinear solutions. It also serves as a confirmation of the gauge choice made in Ref. [24] and used in this work.

Secondly, the anomalous charge defined above inherits a feature from the holographic model. In effective models, normal and anomalous charge are both constant and separable, see e.g. Ref. [13]. In the holographic model, the anomalous charge, as well as the normal charge, depends on the holographic coordinate ρ. Only the sum of the two is a constant. It is known that the holographic coordinate plays the role of renormalization group (RG) scale. It is interesting to analyze the variation of $n_{\rm anom}$ along the RG scale: since $\chi=0$ at both horizon and boundary, we conclude that $n_{\rm anom}$ vanishes in the IR and UV limits. At the intermediate scale, $n_{\rm anom}>0$. To construct an effective model based on holographic theory, we would need to integrate out the holographic coordinate from UV to a certain cutoff scale in the middle. The resultant effective anomalous charge is not expected to be a simple product Bk, in contrast to effective models.

Finally, we discuss the two exotic MCDW states at $B/(\pi T)^2=15$ and their relation with axial anomaly. One state has $\mu=0$, but $n\neq0(k\neq0)$. According to the definition (19), A_t' has at least one zero. We confirm this by plotting $A_t'(\rho)$ in Fig. 8.

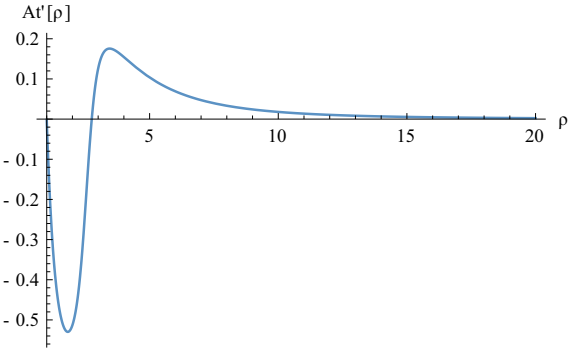

Fig. 8. (color online) $A_t'(\rho)$ at $B/(\pi T)^2=15$. The positive and negative contributions in $\int {\rm d}\rho A_t'(\rho)$ cancel out, giving a vanishing μ. There is one zero of $A_t'(\rho)$, at which $n_{\rm norm}=0$ and $n_{\rm anom}=Bk\left(2\chi^2-\chi^4\right)$. This explains why n and k have the same sign.

Naively, the axial anomaly is not relevant for $\mu=0$. This is not true: although the integration of $A_t'(\rho)$ vanishes, the integration of the WZ term is non-vanishing, which contributes to the thermodynamics. Mathematically, the contributions from the DBI and WZ terms take the following form:

$$\Omega^n_{\rm DBI}/V\neq-\int {\rm d}\rho A_t' n_{\rm norm},\quad \Omega^n_{\rm WZ}/V=-\int {\rm d}\rho A_t' n_{\rm anom}. \tag{27}$$

We use the superscript n to indicate that they are contributions from density. The WZ term is a simple coupling between chemical potential and $n_{\rm anom}$, while the DBI term cannot be written as a simple coupling between chemical potential and $n_{\rm norm}$ due to the nonlinear dependence of DBI action on A_t'. If this were true, we could combine the two terms by using $n_{\rm norm}+n_{\rm anom}=$constant, giving a vanishing contribution because $\mu=\int {\rm d}\rho A_t'=0$. However, due to the different nature of anomalous charge and normal charge, anomaly can still play a role even at $\mu=0$.

The other two states have $n=0$ and $k=0$ respectively. Although they lie close in μ numerically, we can argue that they are different states. For states with $n=0$, we need $n_{\rm norm}$ and $n_{\rm anom}$ to cancel each other. Since $n_{\rm norm}$ is in general nonvanishing for arbitrary ρ, $n_{\rm anom}$ must also be nonvanishing. Thus we cannot have a state with $n=0$ and $k=0$ simultaneously. The state with $n=0$ and $k\neq0$ is still related to axial anomaly as we need anomalous charge to cancel normal charge. The state with $k=0$ and $n\neq0$ is homogeneous, thus it should reduce to the χSB case. In Fig. 9 we show a comparison of density and chiral condensate between the MCDW phase and χSB phase. It confirms a continuous merging of the two phases. Combining with Fig. 7, we suggest that the χSB phase may be replaced by the MCDW phase.

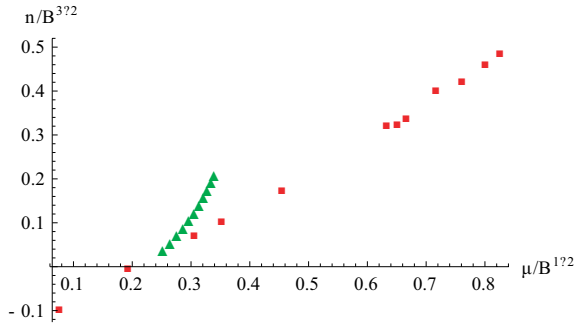

Fig. 9. (color online) $n/B^{3/2}$ versus $\mu/B^{1/2}$ at $B/(\pi T)^2=15$ for the small k branch of the MCDW phase (red squares) and the χSB phase (green triangles). At $\mu/B^{1/2}\simeq0.25$, the density corresponding to the two phases merges, suggesting a second order phase transition. The critical value of μ agrees with the $k=0$ state of MCDW phase in Fig. 6 and also the free energy comparison in Fig. 7.

5 Summary and outlook

We have explored the end point of the spiral instability studied in Ref. [24]. We find the end point solution contains both chiral condensate and pseudoscalar condensate, analogous to the magnetized chiral density wave phase in the literature [13]. The MCDW phase contains two branches of solutions, in accordance with the number of unstable modes found in Refs. [24, 40]. Within each branch, the momentum k can take continuous values. Minimizing the free energy with respect to

k gives the thermodynamically preferred state. We find that for not large B, the large k branch of the MCDW phase is the preferred state out of the two branches. In this case, there is a critical μ, beyond which the MCDW phase dominates over the χS and χSB phases. For large B, the small k branch becomes preferred out of the two branches for a wide range of μ. At sufficient large μ, the MCDW phase becomes dominant over the χS and χSB phases.

We also give a holographic definition of anomalous charge. The anomalous charge in the holographic model varies along RG flow. In particular, it vanishes in the IR and UV limits in our model, but is finite at the intermediate scale. The sum of anomalous and normal charge is constant along the RG flow.

We also find an exotic state of MCDW phase at large B and vanishing μ. Surprisingly, axial anomaly still plays a role at vanishing μ, leading to the formation of spiral phase. The reason is that normal charge and anomalous charge respond to μ differently. The free energy can be lowered by forming a nonvanishing sum of the two.

This work can be extended in a few directions. First of all, we focus on finite density states in this work. To have a complete study of the phase diagram, we still need zero-density states. Homogeneous zero-density states have been studied in Ref. [31]. It would be interesting to see whether the MCDW phase exists at zero density. A closely related question is to find out whether a magnetized kink solution can be realized in holographic models and how it may change the phase diagram.

Secondly, at strong magnetic field and finite μ or finite axial chemical potential μ_5, the ground state is conjectured to be the chiral magnetic spiral phase. Rather than longitudinal spiral (along the magnetic field), it is characterized by a transverse spiral. While the case with $\mu_5 \neq 0$ is confirmed in holographic model studies [29, 41, 42], the case with $\mu \neq 0$ is not found in the same studies. It is desirable to have an independent check within our model.

Last but not least, it would also be interesting to explore the transports of the MCDW phase. Since the MCDW phase breaks both chiral symmetry and translational symmetry, it would be interesting to study the corresponding Nambu-Goldstone modes, and moreover the hydrodynamics in the MCDW phase background. We leave these for future studies.

S.L. is grateful to Gaoqing Cao, Yoshimasa Hidaka and Keun-Young Kim for useful discussions.

References

1 S. P. Klevansky and R. H. Lemmer, Phys. Rev. D, **39**: 3478 (1989).
2 K. G. Klimenko, Theor. Math. Phys., **90**: 1 (1992) [Teor. Mat. Fiz., **90**: 3 (1992)]
3 V. P. Gusynin, V. A. Miransky, and I. A. Shovkovy, Nucl. Phys. B, **462**: 249 (1996)
4 G. S. Bali, F. Bruckmann, G. Endrodi, Z. Fodor, S. D. Katz, S. Krieg, A. Schafer, and K. K. Szabo, JHEP, **1202**: 044 (2012)
5 G. S. Bali, F. Bruckmann, G. Endrodi, Z. Fodor, S. D. Katz, and A. Schafer, Phys. Rev. D, **86**: 071502 (2012)
6 E. Nakano and T. Tatsumi, Phys. Rev. D, **71**: 114006 (2005)
7 D. Nickel, Phys. Rev. Lett., **103**: 072301 (2009)
8 D. Nickel, Phys. Rev. D, **80**: 074025 (2009)
9 M. G. Alford, J. A. Bowers, and K. Rajagopal, Phys. Rev. D, **63**: 074016 (2001)
10 T. Kojo, Y. Hidaka, L. McLerran, and R. D. Pisarski, Nucl. Phys. A, **843**: 37 (2010)
11 M. Buballa and S. Carignano, Prog. Part. Nucl. Phys., **81**: 39 (2015)
12 I. E. Frolov, V. C. Zhukovsky, and K. G. Klimenko, Phys. Rev. D, **82**: 076002 (2010)
13 T. Tatsumi, K. Nishiyama, and S. Karasawa, Phys. Lett. B, **743**: 66 (2015)
14 E. J. Ferrer and V. de la Incera, Nucl. Phys. B, **931**: 192 (2018)
15 E. J. Ferrer and V. de la Incera, Phys. Lett. B, **769**: 208 (2017)
16 G. Cao and A. Huang, Phys. Rev. D, **93**: no. 7, 076007 (2016)
17 E. J. Ferrer, V. de la Incera, and A. Sanchez, Acta Phys. Polon. Supp., **5**: 679 (2012)
18 D. T. Son and M. A. Stephanov, Phys. Rev. D, **77**: 014021 (2008)
19 M. Eto, K. Hashimoto, and T. Hatsuda, Phys. Rev. D, **88**: 081701 (2013)
20 G. Basar, G. V. Dunne, and D. E. Kharzeev, Phys. Rev. Lett., **104**: 232301 (2010)
21 T. Brauner and N. Yamamoto, JHEP, **1704**: 132 (2017)
22 V. A. Miransky and I. A. Shovkovy, Phys. Rept., **576**: 1 (2015)
23 D. E. Kharzeev, K. Landsteiner, A. Schmitt, and H. U. Yee, Lect. Notes Phys., **871**: 1 (2013)
24 D. E. Kharzeev and H. U. Yee, Phys. Rev. D, **84**: 125011 (2011)
25 S. K. Domokos and J. A. Harvey, Phys. Rev. Lett., **99**: 141602 (2007)
26 M. Ammon, J. Leiber, and R. P. Macedo, JHEP, **1603**: 164 (2016)
27 S. Nakamura, H. Ooguri, and C. S. Park, Phys. Rev. D, **81**: 044018 (2010)
28 H. Ooguri and C. S. Park, Phys. Rev. Lett., **106**: 061601 (2011)
29 K. Y. Kim, B. Sahoo, and H. U. Yee, JHEP, **1010**: 005 (2010)
30 J. de Boer, B. D. Chowdhury, M. P. Heller, and J. Jankowski, Phys. Rev. D, **87**(6): 066009 (2013)
31 N. Evans, A. Gebauer, K. Y. Kim, and M. Magou, JHEP, **1003**: 132 (2010)
32 D. Mateos, R. C. Myers, and R. M. Thomson, Phys. Rev. Lett., **97**: 091601 (2006)
33 D. Mateos, R. C. Myers, and R. M. Thomson, JHEP, **0705**: 067 (2007)
34 S. R. Das, T. Nishioka, and T. Takayanagi, JHEP, **1007**: 071 (2010)
35 C. Hoyos, T. Nishioka, and A. O'Bannon, JHEP, **1110**: 084 (2011)
36 T. G. Lee, E. Nakano, Y. Tsue, T. Tatsumi, and B. Friman, Phys. Rev. D, **92**: no. 3, 034024 (2015)
37 Y. Hidaka, K. Kamikado, T. Kanazawa, and T. Noumi, Phys. Rev. D, **92**: no. 3, 034003 (2015)
38 A. Karch and A. O'Bannon, JHEP, **0711**: 074 (2007)
39 E. d. Guo and S. Lin, Phys. Rev. D, **93**: no. 10, 105001 (2016)
40 E. d. Guo and S. Lin, JHEP, **1701**: 111 (2017)
41 A. Ballon-Bayona, K. Peeters, and M. Zamaklar, JHEP, **1211**: 164 (2012)
42 C. A. B. Bayona, K. Peeters, and M. Zamaklar, JHEP, **1106**: 092 (2011)